Supplementary Information for

Intensified dominance of El Niño-like convection relevant for global atmospheric circulation variations

Fenying Cai [1, 2], Shuheng Lin [3*], Dieter Gerten [1, 2], Song Yang [4, 5*], Xingwen Jiang [6], Zhen Su [1, 7], and Jürgen Kurths [1, 8, 9]

[1] Potsdam Institute for Climate Impact Research (PIK), Member of the Leibniz Association, P.O. Box 60 12 03 D-14412 Potsdam, Germany

[2] Department of Geography, Humboldt-Universität zu Berlin, 10099 Berlin, Germany

[3] Key Laboratory of Humid Subtropical Eco-geographical Process (Ministry of Education), College of Geographical Sciences, Fujian Normal University, 350108 Fuzhou, China

[4] School of Atmospheric Sciences, Sun Yat-sen University, and Southern Marine Science and Engineering Guangdong Laboratory (Zhuhai), 519082 Zhuhai, China

[5] Guangdong Province Key Laboratory for Climate Change and Natural Disaster Studies, Sun Yat-sen University, 519082 Zhuhai, China

[6] Heavy Rain and Drought-Flood Disasters in Plateau and Basin Key Laboratory of Sichuan Province, Institute of Tibetan Plateau Meteorology, China Meteorological Administration, Chengdu, Sichuan 610072, China

[7] Department of Computer Science, Humboldt-Universität zu Berlin, 10099 Berlin, Germany

[8] Department of Physics, Humboldt-Universität zu Berlin, 10099 Berlin, Germany

[9] School of Mathematical Sciences, SCMS, and CCSB, Fudan University, 200433 Shanghai, China

Submitted to ***Nature Climate Change***

November 2024

This PDF file includes:

Supplementary Table S1

Supplementary Figures S1 to S7

Table S1 | List of 23 CMIP6 models.

Model	Institution
ACCESS-CM2	Alfred Wegener Institute, Helmholtz Centre for Polar and Marine Research (AWI), Germany
BCC-CSM2-MR	Beijing Climate Centre, China
CanESM5	Canadian Centre for Climate Modelling and Analysis, Environment and Climate Change Canada, Canada
CESM-WACCM	National Centre for Atmospheric Research (NCAR), Climate and Global Dynamics Laboratory, Boulder, USA
EC-Earth3	EC-Earth consortium, Rossby Center, Swedish Meteorological and Hydrological Institute/SMHI, Norrkoping, Sweden
EC-Earth-Veg	
FOGALS-g3	Chinese Academy of Sciences, Beijing, China
GFDL-CM4	National Oceanic and Atmospheric Administration, Geophysical Fluid Dynamics Laboratory, Princeton, NJ, USA
HadGEM3-GC31-LL	Met Office Hadley Centre, Exeter, UK
HadGEM3-GC31-MM	
IITM-ESM	Centre for Climate Change Research Indian Institute of Tropical Meteorology, Pune, India

INM-CM4-8	Institute for Numerical Mathematics (INM), Russian Academy of Science, Moscow, Russia
INM-CM5-0	
IPSL-CM6A-LR	Institute Pierre Simon Laplace (IPSL), Paris, France
KACE-1-0-G	National Institute of Meteorological Sciences/Korea Meteorological Administration, Climate Research Division, Korea
MIROC6	Japan Agency for Marine-Earth Science and Technology (JAMSTEC), Atmosphere and Ocean Research Institute (AORI), The University of Tokyo, National Institute for Environmental Studies (NIES), and RIKEN Center for Computational Science, Japan
MPI-ESM1-2-HR	Max Planck Institute for Meteorology (MPI-M), Germany
MPI-ESM1-2-LR	
MRI-ESM2-0	Meteorological Research Institute (MRI), Japan
NorESM2-LM	NorESM Climate Modeling Consortium, Norway
NorESM2-MM	NorESM Climate Modeling Consortium, Norway
TaiESM1	Research Center for Environmental Changes, Taiwan, China
UKESM1-0-LL	Met Office Hadley Centre, Exeter, UK

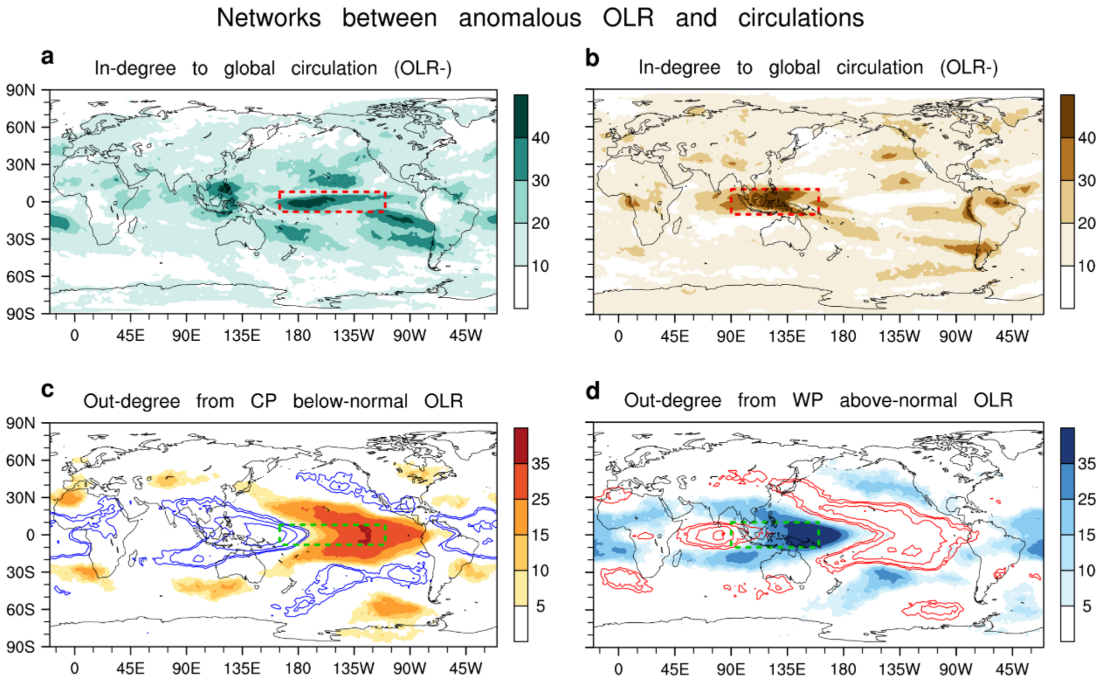

Figure S1. Degree centrality of relevance for global atmospheric circulation variations and for equatorial Pacific anomalous Outgoing Longwave Radiation (OLR). The network results are based on pentad-mean ERA5 OLR and geopotential height at 300 hPa during 1979–2022. In-degree centrality to global anomalous pressure events (units: $\times$ 10,000) summed for **(a)** two networks based on above-normal convection events, and **(b)** two networks based on below-normal convection events. **(c)** Out-degree centrality from above-normal convection events over the equatorial central Pacific, for high-pressure events (shadings; units: $\times$1,000) and low-pressure events (blue contours shown at 10,000, 15,000, 25,000, and 35,000). **(d)** Out-degree centrality from below-normal convection events over the equatorial western Pacific, for low-pressure events (shadings; units: $\times$ 1,000) and high-pressure events (red contours shown at 10,000, 15,000, 25,000, and 35,000). Equatorial western Pacific (10°S–10°N, 90°–160°E) and equatorial central Pacific (10°S–10°N, 170°E–120°W) are outlined by the colored boxes in **(a–d)**.

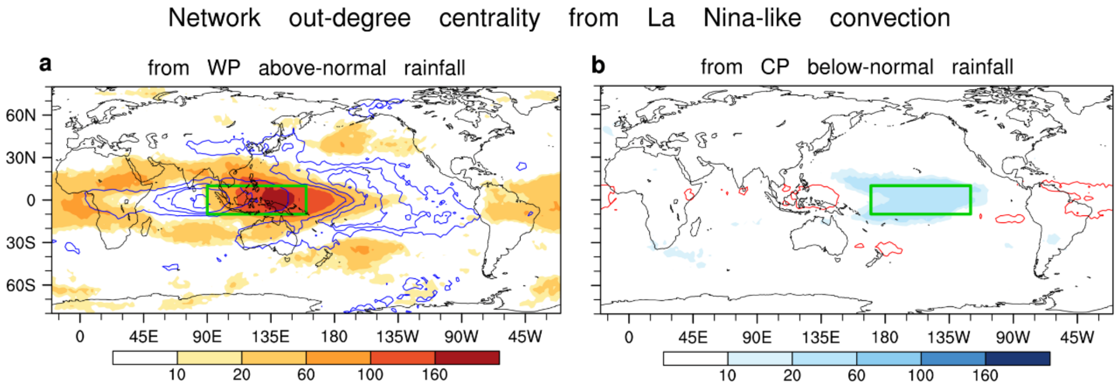

Figure S2. Atmospheric teleconnections linked to La Niña-like convection revealed by network analysis. (a) Out-degree centrality from above-normal rainfall events over the equatorial western Pacific (WP), for high-pressure events (shadings; units: ×100) and low-pressure events (blue contours shown at 2,000, 6,000, 12,000, and 16,000). **(b)** Out-degree centrality from below-normal rainfall events over the equatorial central Pacific (CP), for low-pressure events (shadings; units: ×100) and high-pressure events (red contours shown at 2,000, 6,000, 12,000, and 16,000). All plotted shadings and contours in **(a–b)** are significant because only significant links ($p<0.01$) are retained and used to calculate degree centralities. Equatorial western Pacific (10°S–10°N, 90°–160°E) and equatorial central Pacific (10°S–10°N, 170°E–120°W) are outlined by the green boxes in **(a)** and **(b)**, respectively.

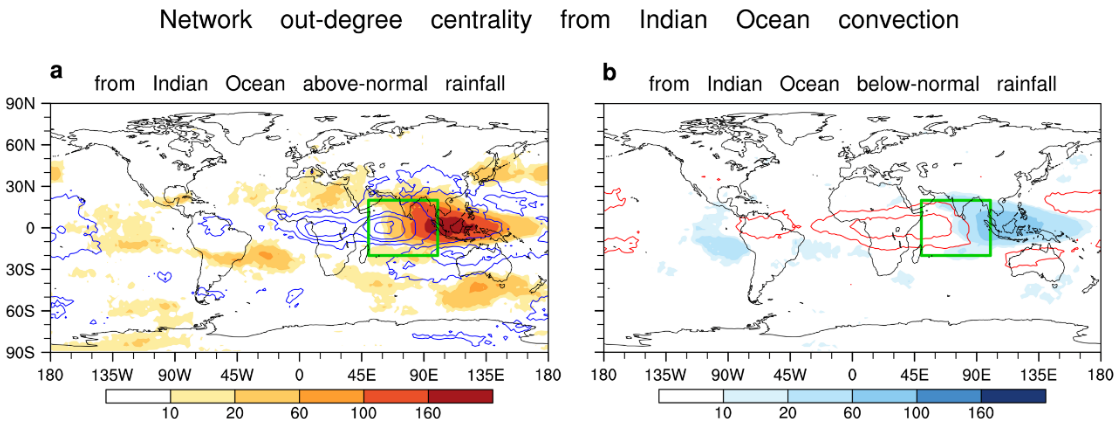

Figure S3. Atmospheric teleconnections linked to Indian Ocean convection anomalies revealed by network analysis. (a) Out-degree centrality from above-normal rainfall events over the tropical Indian Ocean, for high-pressure events (shadings; units: ×100) and low-pressure events (blue contours shown at 2,000, 6,000, 12,000, and 16,000). **(b)** Out-degree centrality from below-normal rainfall events over the tropical Indian Ocean, for low-pressure events (shadings; units: ×100) and high-pressure events (red contours shown at 2,000, 6,000, 12,000, and 16,000). All plotted shadings and contours in **(a–b)** are significant because only significant links ($p<0.01$) are retained and used to calculate degree centralities. Tropical Indian Ocean (20°S–20°N, 50°–100°E) is outlined by the green boxes in **(a)** and **(b)**.

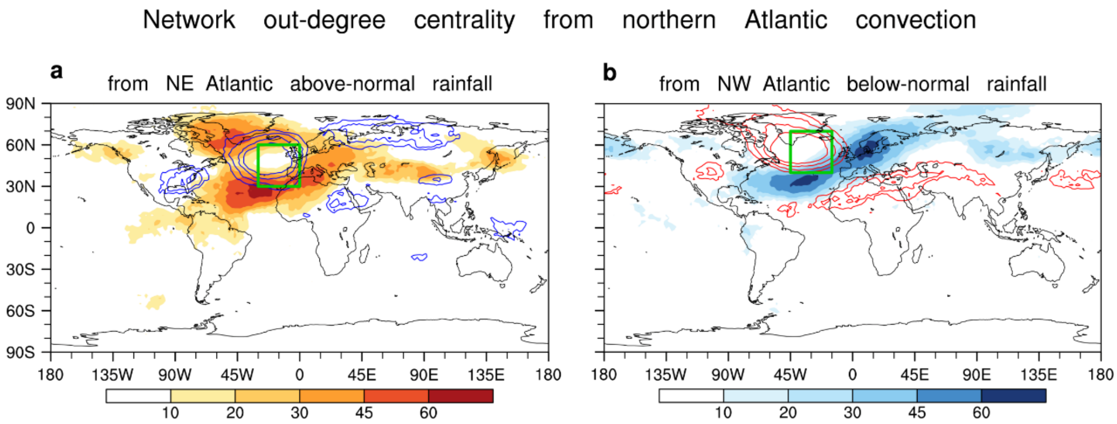

Figure S4. Atmospheric teleconnections linked to North Atlantic convection anomalies revealed by network analysis. (a) Out-degree centrality from above-normal rainfall events over the northeastern Atlantic, for high-pressure events (shadings; units: ×100) and low-pressure events (blue contours shown at 2,000, 3,000, 4,500, and 6,000). **(b)** Out-degree centrality from below-normal rainfall events over the northwestern Atlantic, for low-pressure events (shadings; units: ×100) and high-pressure events (red contours shown at 2,000, 3,000, 4,500, and 6,000). All plotted shadings and contours in **(a–b)** are significant because only significant links ($p<0.01$) are retained and used to calculate degree centralities. Northeastern Atlantic (30°–60°N, 30°W–0°) and northwestern Atlantic (40°–70°N, 45°W–15°W) are outlined by the green boxes in **(a)** and **(b)**, respectively.

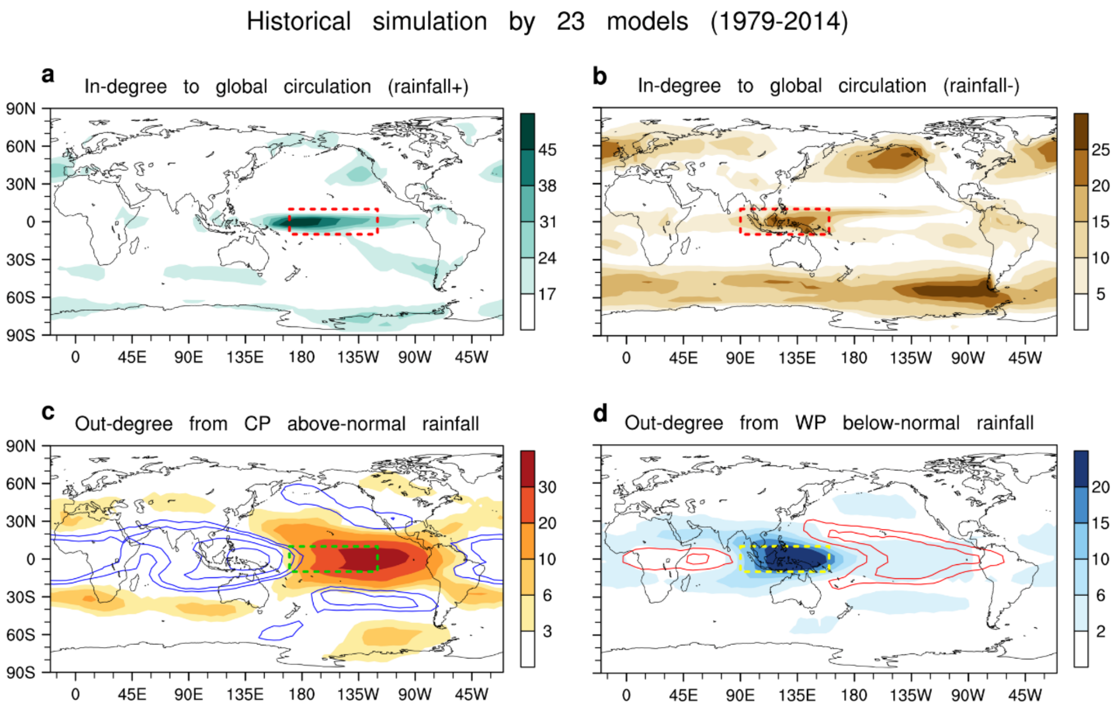

Figure S5. Degree centrality relevant for global atmospheric circulation variations and for equatorial Pacific anomalous rainfall in CMIP6 historical simulations. The network results are based on pentad-mean rainfall and geopotential height at 250 hPa in the historical simulations of 23 CMIP6 models during 1979–2014. In-degree centrality to global anomalous pressure events (units: ×1,000) summed for **(a)** two networks based on above-normal rainfall events, and **(b)** two networks based on below-normal rainfall events. **(c)** Out-degree centrality from above-normal rainfall events over the equatorial central Pacific, for high-pressure events (shadings; units: ×100) and low-pressure events (blue contours shown at 800, 1,200, 2,000, and 3,000). **(d)** Out-degree centrality from below-normal rainfall events over the equatorial western Pacific, for low-pressure events (shadings; units: × 100) and high-pressure events (red contours shown at 600, 900, 1,500, and 2,000). Equatorial western Pacific (10°S–10°N, 90°–160°E) and equatorial central Pacific (10°S–10°N, 170°E–120°W) are outlined by the colored boxes in **(a–d)**.

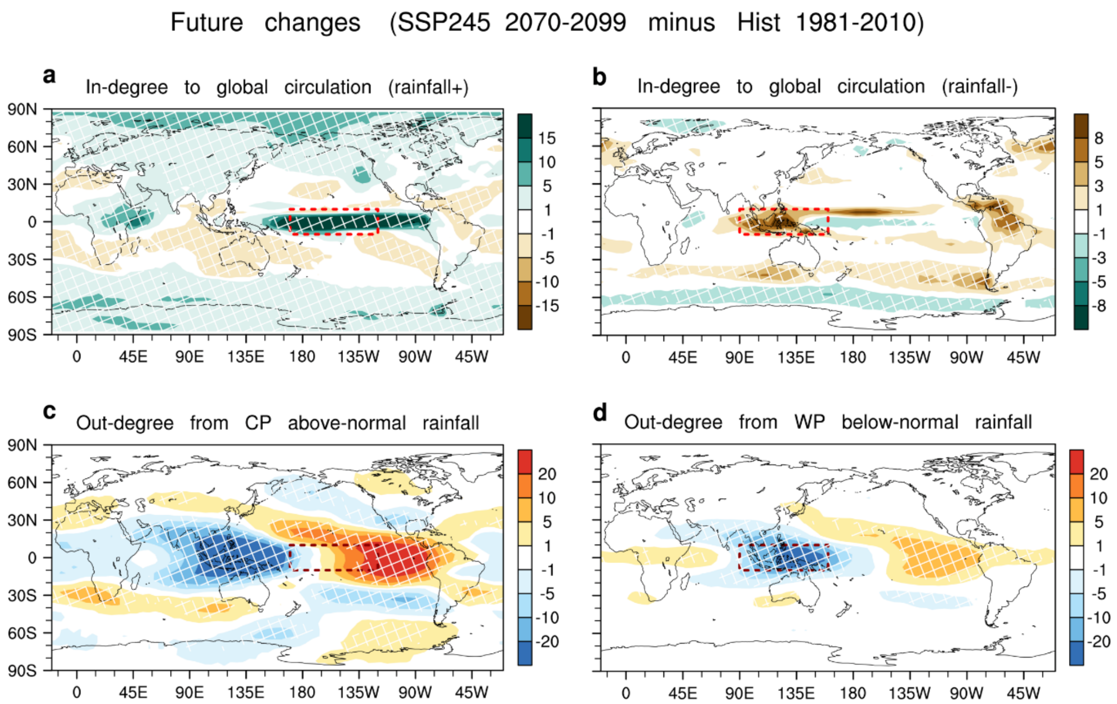

Figure S6. Projected long-term changes in degree centrality relevant for global atmospheric circulation variations and for equatorial Pacific anomalous rainfall by CMIP6 models under the SSP245 scenario. Projected long-term changes are calculated as the differences between the period 2070–2099 under the SSP245 scenario and the period 1981–2010 under the historical simulations. Projected changes of in-degree centrality to global anomalous pressure events (units: $\times$1,000) summed for **(a)** two networks based on above-normal rainfall events, and **(b)** two networks based on below-normal rainfall events. Projected changes in out-degree centrality differences (shadings; units: $\times$100) between networks based on high-pressure events and low-pressure events, from **(c)** above-normal rainfall events over the equatorial central Pacific, and from **(d)** below-normal rainfall events over the equatorial western Pacific. Hatched areas in **(a–d)** show where at least 18 models (> 81% of the total 22 models) project the changes with same signs. Equatorial western Pacific (10°S–10°N, 90°–160°E) and equatorial central Pacific (10°S–10°N, 170°E–120°W) are outlined by the colored boxes in **(a–d)**. The 22 models for the SSP245 scenario are as same as those under the SSP 585 scenario, but not including HadGEM3-GC31-MM.

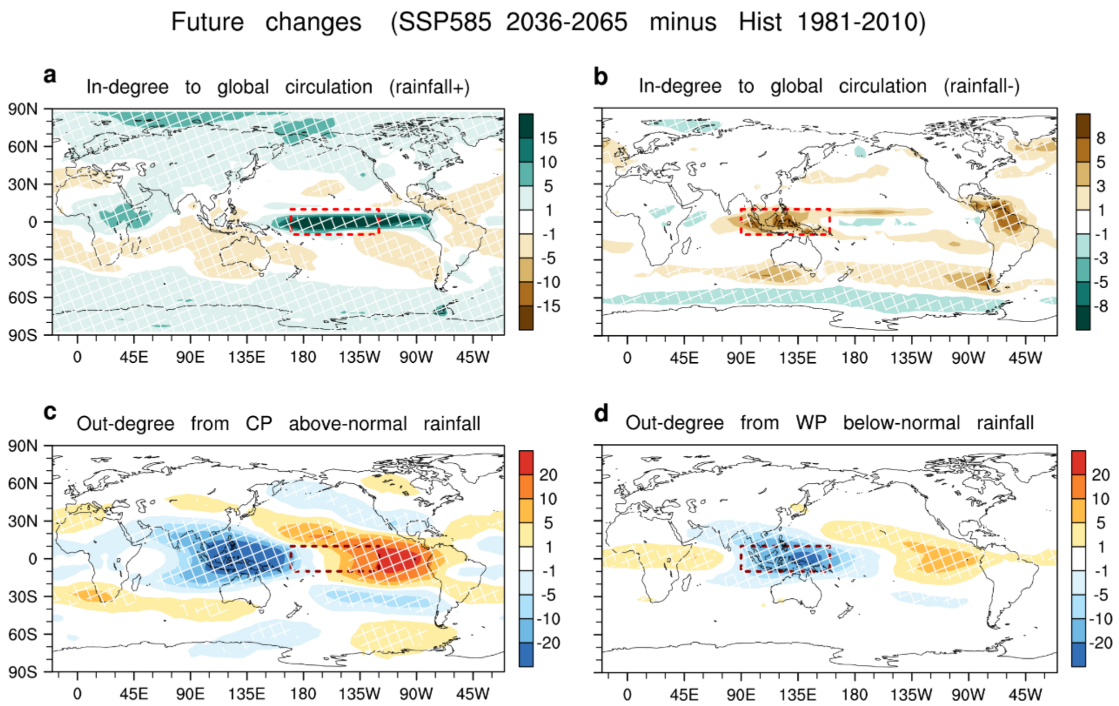

Figure S7. Projected mid-term changes in degree centrality relevant for global atmospheric circulation variations and for equatorial Pacific anomalous rainfall by CMIP6 models. Projected mid-term changes are calculated as the differences between the period 2036–2065 under the SSP585 scenario and the period 1981–2010 under the historical simulations. Projected changes of in-degree centrality to global anomalous pressure events (units: ×1,000) summed for **(a)** two networks based on above-normal rainfall events, and **(b)** two networks based on below-normal rainfall events. Projected changes in out-degree centrality differences (shadings; units: ×100) between networks based on high-pressure events and low-pressure events, from **(c)** above-normal rainfall events over the equatorial central Pacific, and from **(d)** below-normal rainfall events over the equatorial western Pacific. Hatched areas in **(a–d)** show where at least 19 models (> 82% of the total 23 models) project the changes with same signs. Equatorial western Pacific (10°S–10°N, 90°–160°E) and equatorial central Pacific (10°S–10°N, 170°E–120°W) are outlined by the colored boxes in **(a–d)**.